GEOPHYSICAL RESEARCH LETTERS, VOL. 40, 6181–6185, doi:10.1002/2013GL058403, 2013

Marginal instability and deep cycle turbulence in the eastern equatorial Pacific Ocean

W. D. Smyth[1] and J. N. Moum[1]

Received 29 October 2013; revised 26 November 2013; accepted 27 November 2013; published 8 December 2013.

[1] Deep cycle mixing in the cold tongue of the equatorial Pacific Ocean is associated with a mean flow regime in which the gradient Richardson number *Ri* (a ratio of stratification to shear that affects the evolution of turbulence) fluctuates about a critical value near $\frac{1}{4}$. This is the state of *marginal instability* (MI), a stable equilibrium between forcing by the trade winds (which works to reduce *Ri*) and turbulence (which works to increase *Ri*). Besides providing insight into the physics of deep cycle turbulence, MI is easily recognized in moored records of currents and density, and may therefore provide a valuable indicator of turbulence in historical data where direct turbulence measurements were not made. In this initial study, the seasonal cycle of MI is described. MI is present for 9 months of the year but disappears in March, April, and May, consistent with the recently discovered springtime minimum of equatorial turbulence. **Citation:** Smyth, W. D., and J. N. Moum (2013), Marginal instability and deep cycle turbulence in the eastern equatorial Pacific Ocean, *Geophys. Res. Lett.*, *40*, 6181–6185, doi:10.1002/2013GL058403.

1. Introduction

[2] In the eastern equatorial Pacific and Atlantic Oceans, currents driven by the trade winds diverge due to the Earth's rotation, bringing cool water from the thermocline nearer to the surface. In the ∼100 m thick shear layer between the surface and the equatorial undercurrent (EUC; see Figure 1a), strong turbulence mixes the upwelled thermocline waters with warm surface water [*Moum et al.*, 2009, 2013], reducing sea surface temperature (SST). The resulting "cold tongues" are regions of rapid heat uptake by the ocean and are therefore crucial to the global climate [e.g., *de Szoeke and Xie*, 2008; *Xie*, 2013].

[3] SST is influenced directly by turbulence in the surface mixed layer (SML; see Figure 1d), in which density varies little from its surface value and vertical motions driven by wind and surface cooling are therefore hindered only slightly by gravity. Early measurements in the Pacific cold tongue revealed a new phenomenon: strong turbulence extending for several tens of meters into the stratified fluid *beneath* the SML. Despite its remoteness from diurnal surface forcing, this turbulence exhibits a distinct diurnal cycle, and it has therefore come to be known as the "deep cycle" (DC) [*Gregg et al.*, 1985; *Moum and Caldwell*, 1985].

[4] This note describes initial results from a long-term survey of DC variability. We describe a new diagnostic, the property of marginal instability (MI) [*Thorpe and Liu*, 2009], and explore its relationship with DC turbulence. While it does not predict the strength of turbulence, MI identifies flow regimes in which turbulence is strong enough to attain equilibrium with its forcing (the trade winds, in this case). In section 2, we discuss the statistics of the gradient Richardson number in the DC layer and define MI in detail. In section 3, we analyze the seasonal cycle using 5 years of data from the TAO (Tropical Ocean and Atmosphere) mooring at 0°N–140°W [*McPhaden*, 1995] and compare the results with measurements of DC turbulence from fast thermistors mounted on the same mooring [*Moum and Nash*, 2009; *Perlin and Moum*, 2012].

2. The Deep Cycle, the Richardson Number, and the Marginal Instability

[5] The energy source for DC turbulence in the region above the undercurrent core is the vertical shear of the horizontal current whose zonal and meridional components are written as U and V, respectively. The squared magnitude of the shear is defined by $S^2 = (\partial U/\partial z)^2 + (\partial V/\partial z)^2$. Countering the shear is the stabilizing effect of gravity, quantified by the squared buoyancy frequency $N^2 = -(g/\rho)\partial\rho/\partial z$, where ρ is density and g is gravitational acceleration. The gradient Richardson number is the ratio of these: $Ri = N^2/S^2$. Values $\ll 1$ indicate that instability and turbulence are likely, since shear is sufficient to do the work against gravity needed to initiate vertical motions.

[6] In this section, we illustrate the DC using measurements made at 0°N–140°W during boreal fall, 2008 (Figure 1). Profiles of density and shear microstructure (with vertical resolution near 1 cm) were obtained approximately eight times per hour. Currents were measured by a combination of ADCPs (acoustic Doppler current profilers) with resolution 2 m (twice the resolution used in previous cruises to this location) [see *Moum et al.*, 2009 for further details].

[7] This was a La Niña period; hence the undercurrent was relatively strong (Figure 1a, red). Tropical instability waves [*Kennan and Flament*, 2000; *Lyman et al.*, 2007], evident in the broad variability of the meridional current near the surface (Figure 1a, blue), added to the shear of the zonally directed undercurrent [*Moum et al.*, 2009]. From 20 m down to 70 m depth, both S^2 and N^2 increased by an order of magnitude (Figure 1b), but did so in such close proportion to one another that their ratio, *Ri*, varied by less than a factor of two (Figure 1c). Associated with these mean flow properties was the DC: strong turbulence

Additional supporting information may be found in the online version of this article.

[1]College of Oceanic and Atmospheric Sciences, Oregon State University, Corvallis, Oregon, USA.

Corresponding author: W. D. Smyth, College of Oceanic and Atmospheric Sciences, Oregon State University, Corvallis, OR 97331, USA. (smyth@coas.oregonstate.edu)

0094-8276/13/10.1002/2013GL058403

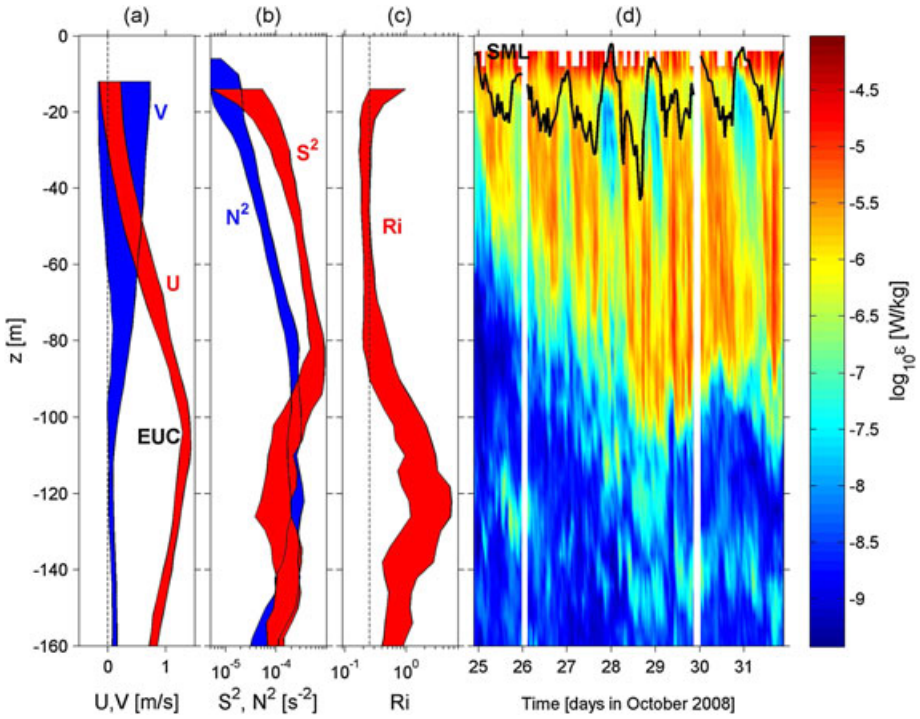

Figure 1. Hourly averaged currents (a) U and V, (b) squared shear S^2 and buoyancy frequency N^2, and (c) Richardson number Ri. In Figure 1a, "EUC" indicates the depth of the equatorial undercurrent. Measurements were made over 7 days in boreal fall, 2008. Each filled curve represents the middle 50% of hourly averages. Dashed lines indicate zero current in Figure 1a; $Ri = \frac{1}{4}$ in Figure 1c. (d) At the right is the time-depth dependence of the turbulent kinetic energy dissipation rate, ϵ [*Moum and Rippeth*, 2008], over the same period. Vertical white bands indicate data gaps. The solid curve is the base of the SML, defined by a density change of 0.01 kg m^{-3} from the surface.

extending for many tens of meters below the SML base (Figure 1d) while retaining the diurnal imprint of the surface forcing. Most observations of the DC to date have been made in the eastern Pacific cold tongue. Observations in the Atlantic cold tongue have shown a similar enhancement of turbulence below the SML [*Hummels et al.*, 2013], though the diurnal cycle is less clearly defined, possibly due to insufficient temporal resolution in the data.

[8] Of particular importance here is the uniformity of Ri over much of the DC layer, with a typical value in the neighborhood of $\frac{1}{4}$. The value $Ri = \frac{1}{4}$ (Figure 1c) arises in several contexts. For example, modal instabilities that drive a stratified, parallel shear flow toward the turbulent state exist only if the minimum Ri is less than $\frac{1}{4}$ [*Miles*, 1961]. Fully-developed, homogeneous turbulence in a mean flow with uniform S^2 and N^2 grows if $Ri < \frac{1}{4}$, decays if $Ri > \frac{1}{4}$, and reaches equilibrium if $Ri = \frac{1}{4}$ [*Rohr et al.*, 1988]. $Ri \sim \frac{1}{4}$ is therefore a natural equilibrium state for strong turbulence in stratified shear flow.

[9] MI exists when, over a spatially and temporally extended region, the mean flow is close to a boundary in parameter space between disturbance growth and decay. $Ri = \frac{1}{4}$ is a familiar approximation for this boundary, and we use it freely with the awareness that the true boundary can depend on other factors such as Reynolds number and ambient turbulence levels [e.g., *Rohr et al.*, 1988; *Shih et al.*, 2000; *Thorpe and Liu*, 2009; *Thorpe et al.*, 2013]. Also, while $Ri = \frac{1}{4}$ is the critical state for the initiation of shear instability, the resulting turbulence persists up to a higher Ri value, typically near $\frac{1}{3}$ [*Thorpe*, 1973; *Smyth and Moum*,

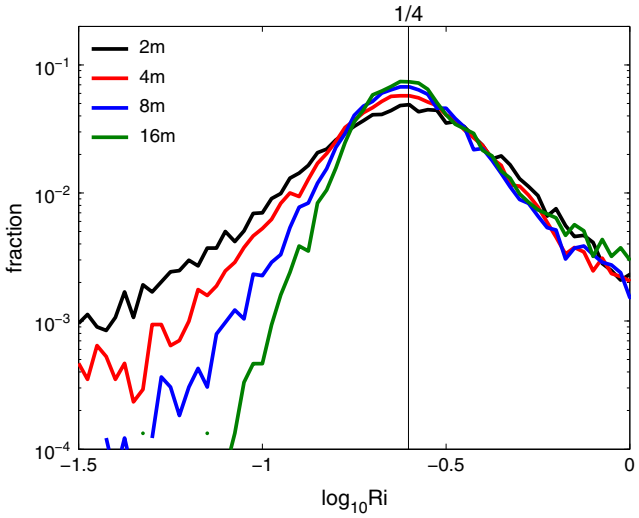

Figure 2. Distribution of Ri below the SML from highly resolved ADCP and microstructure profiler observations made in fall 2008 at 0°N–140°W (as in Figure 1c). Statistics are computed in the layer –70 m < z < –20 m. The vertical derivatives, currents, and density that form Ri are computed as centered differences with various spacings as specified in the legend. The vertical line indicates $Ri = \frac{1}{4}$. The peak at $Ri = \frac{1}{4}$ is independent of resolution, but finer resolution reveals increased incidence of $Ri < \frac{1}{4}$.

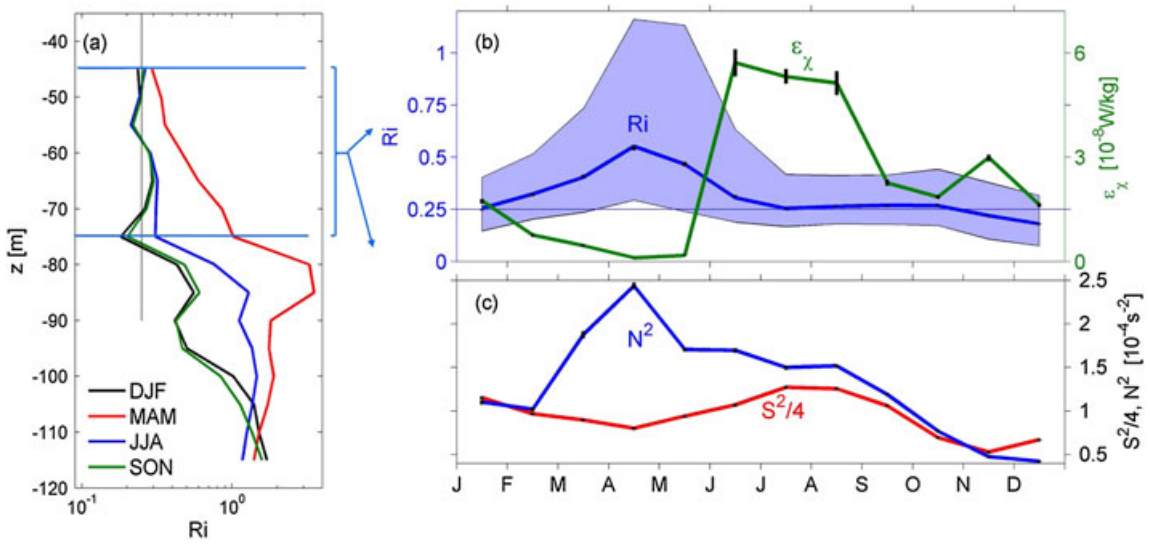

Figure 3. The seasonal cycle of MI and DC turbulence. (a) Three-month medians of hourly averaged *Ri* profiles during 23 September 2005 to 10 September 2010 at 0°N–140°W. (b) Blue: Monthly median of hourly *Ri* measurements between $z = –45$ m and $z = –75$ m. Shading represents the upper and lower quartiles. Green: Median of ϵ_χ in the same depth range. (c) Median hourly measurements of S^2 and N^2. Error bars, visible only for ϵ_χ, indicate 95% bootstrap confidence limits on the median.

2000]. The possibility that the upper equatorial Pacific might exhibit MI was first raised by *Thorpe and Liu* [2009] based on a reinterpretation of the stability analyses of *Sun et al.* [1998].

[10] In the MI state, even a small perturbation can reduce *Ri* locally to an unstable value. The resulting turbulence acts to increase *Ri*, restoring stability. Whereas occurrences of $Ri < \frac{1}{4}$ are often small in spatial extent and duration, and may therefore not be resolved in observations, MI is a robust property of the mean flow and relatively easy to detect. To illustrate this, we first compute *Ri* by differencing velocity and density values in adjacent 2 m bins (Figure 2, black curve). Following this, the spacing was repeatedly doubled (red, blue, and green curves). Spacings of 4 m and 8 m represent standard ADCP resolution, while 16 m is typical of moored current meters and large-scale models. The peak at $\frac{1}{4}$ signifies MI and dominates the distribution regardless of resolution. The effect of resolution lies in the skewness; with finer resolution one sees more frequent occurrences of $Ri < \frac{1}{4}$, representing the small-scale instabilities that maintain turbulence.

[11] MI is an example of a forced-dissipative system displaying scale-invariant behavior. A vivid illustration was provided by *Bak et al.* [1987]. Imagine that sand is poured steadily at a point to form a sandpile. The critical slope or angle of repose is maintained on average by sporadic small avalanches. Here the trade winds play the role of the sand source, forcing the zonal current system. The critical state $Ri = \frac{1}{4}$ is analogous to the angle of repose, and the "avalanches" are turbulent eddies.

3. The Seasonal Cycle

[12] We have seen anecdotal evidence that MI can occur together with DC turbulence, but this does not demonstrate a causal connection between the two phenomena. The next step is test for the existence of MI when DC turbulence is *not* active; if the two phenomena are causally related, then MI should vanish when the DC does. Recent measurements have shown that near-surface turbulence at this site varies seasonally, with a marked decrease in boreal spring [*Moum et al.*, 2013]. We now show that this is also true of turbulence in the DC layer, and moreover that MI vanishes at the same time.

[13] We examine the seasonal variability of MI over a 5 year period (23 September 2005 to 10 September 2010) using measurements of temperature made at the TAO mooring at 0°N, 140°W, and of velocity on a separate mooring about 18 km away. These were gridded with spacings of 5 m in the vertical and 1 h in time, then differenced and combined to form S^2, N^2, and *Ri* as defined in section 2. Because salinity measurements are sparse and the saline contribution to density stratification in this region is minor, density needed for N^2 was computed from temperature measurements alone (See "supporting information" for an analysis of uncertainties due to salinity effects and the spatial separation of the moorings. Neither effect alters our conclusions). The median was computed from all values falling into each of four 3 month intervals representing the seasons: boreal summer (identified here as June through August), fall (September through November), winter (December through February), and spring (March through May).

[14] Despite wide variations in currents and stratification, the MI regime below the SML is a remarkably consistent feature. MI is evident during three seasons (Figure 3a). In boreal summer, fall, and winter, between $z = –45$ m (the upper limit of reliable current measurements) and $z = –75$ m, the median *Ri* remained in the range 0.2–0.3, i.e., about half of all 1 h, 5 m *Ri* values were in the unstable regime. The structure in boreal spring was distinctly different: *Ri* increased with depth to 85 m and showed no evidence of MI.

[15] The relationship between the annual cycles of the MI layer and DC turbulence is seen explicitly in monthly median values covering the DC layer (Figures 3b and 3c).

Medians of N^2, S^2, and *Ri* were computed as above but over individual months rather than seasons and over the depth range $-75 \leq z \leq -45$ m. Values of the turbulent kinetic energy dissipation rate measured by the χpods, ϵ_χ [*Perlin and Moum*, 2012], measured at irregular depths in the range -75 m $\leq z <\leq 45$ m over various deployments in 2005–2010 were averaged into 15 min bins, then the median was computed for each month. For further details see *Moum et al.* [2013], who computed the seasonal variation of the near-surface turbulent heat flux. Here we use data from the same χpod deployments to explore turbulent dissipation in the DC layer.

[16] In boreal spring, ϵ_χ is seen to decrease by nearly two orders of magnitude, coincident with a pronounced rise in *Ri* as seen in Figure 3a. Through the other 9 months of the year, MI is evident: *Ri* values cluster just above $\frac{1}{4}$, with over 25% of values lying below $\frac{1}{4}$. In spring, median *Ri* increases while the tendency to cluster about the median decreases. In April, the lower quartile exceeds $\frac{1}{4}$, indicating that less than 25% of values are in the unstable range. These observations confirm that DC turbulence and the MI regime vanish together in boreal spring.

[17] The seasonal cycle of *Ri* reflects changes in both stratification and shear (Figure 3c). The springtime maximum in *Ri* is produced by a combination of strong stratification and weak shear in the DC layer. In June through August, shear increases while stratification remains weak, reducing *Ri* and driving the strongest turbulence of the year (Figure 3b). This turbulence works to erode the stratification that accumulated in the DC layer during spring (though the April–May decrease in N^2 precedes the May–June increase in ϵ_χ, suggesting that stratification is influenced by effects other than local turbulence). By November, shear, stratification, and turbulence are all reduced, while *Ri* remains near $\frac{1}{4}$.

4. Discussion

[18] The tendency of *Ri* in the DC layer to fluctuate about a value near $\frac{1}{4}$ over an extended region of depth and time signifies marginal instability. We have shown that the seasonal cycle of mixing described by *Moum et al.* [2013] extends to the DC layer and is associated with MI. MI varies seasonally in a manner consistent with shear-driven turbulence; MI and DC mixing exist together during boreal summer, fall, and winter and vanish together in spring.

[19] The MI property of turbulence is not associated with planetary rotation. It may therefore be evident not just at the equator but wherever stratified shear flow is driven by sufficiently strong and steady forcing [e.g., *Thorpe and Liu*, 2009].

[20] Through the MI property, statistics of the *Ri* profile give a clear indication of the *existence* of turbulence, though not of its strength. If the opposing effects of large-scale forcing and turbulence are strong enough, they will drive *Ri* to $\frac{1}{4}$. Beyond that point, further increases in forcing/turbulence have no effect, and *Ri* therefore has no further value as a turbulence diagnostic. This is clear from Figure 3b, where the monthly mean dissipation varies by an order of magnitude during the months when MI is evident. (The critical Richardson number is a property of sheared, stratified turbulence in the same sense that the angle of repose is a property of sand. Its value tells us nothing about the flux of energy (or sand) through the system, except that it exceeds the minimum necessary to achieve equilibrium).

[21] Our analysis of the variability of MI has focused on 5 years of observations at a single site, chosen only because χpod measurements are available to demonstrate the MI-DC relationship. The TAO mooring array [*McPhaden*, 1995] has delivered current and density measurements at longitudes spanning the equatorial oceans, in some cases going back to the 1980s. Ongoing analysis of this data will reveal MI variability, both with longitude and over multiple decades. Using MI as a proxy, we will gain a qualitative first look at DC variability over monsoonal, annual, El Niño-Southern Oscillation, and possibly interdecadal periods. In years to come, extensions of the χpod observation program described above will make these results quantitative.

[22] **Acknowledgments.** This paper benefited from critical readings by Sally Warner, Aurelie Moulin and two anonymous reviewers, and from auxiliary analyses by Sally Warner. Funding was provided by the National Science Foundation via grants OCE1030772, OCE0424133, OCE0728365, and OCE1256620.

[23] The Editor thanks two anonymous reviewers for their assistance in evaluating this paper.

References

Bak, P., C. Tang, and K. Wiesenfeld (1987), Self-organized criticality: An explanation of 1/*f* noise, *Phys. Rev. Lett.*, *59*, 381–384.

de Szoeke, S., and S.-P. Xie (2008), The tropical eastern Pacific seasonal cycle: Assessment of errors and mechanisms in IPCC AR4 coupled ocean-atmosphere general circulation models, *J. Clim.*, *21*, 2573–2590.

Gregg, M., H. Peters, J. Wesson, N. Oakey, and T. Shay (1985), Intensive measurements of turbulence and shear in the equatorial undercurrent, *Nature*, *318*, 140–144.

Hummels, R., M. Dengler, and B. Bourlès (2013), Seasonal and regional variability of upper ocean diapycnal heat flux in the Atlantic cold tongue, *Prog. Oceanogr.*, *111*, 52–74.

Kennan, S., and P. Flament (2000), Observations of a tropical instability vortex, *J. Phys. Oceanogr.*, *30*, 2277–2301.

Lyman, J., G. Johnson, and W. Kessler (2007), Distinct 17- and 33-day tropical instability waves in subsurface observations, *J. Phys. Oceanogr.*, *37*, 885–872.

McPhaden, M. (1995), The tropical atmosphere ocean array is completed, *Bull. Am. Meteorol. Soc.*, *76*, 739–741.

Miles, J. (1961), On the stability of heterogeneous shear flows, *J. Fluid Mech.*, *10*, 496–508.

Moum, J., and D. Caldwell (1985), Local influences on shear flow turbulence in the equatorial ocean, *Science*, *230*, 315–316.

Moum, J., R.-C. Lien, A. Perlin, J. Nash, M. Gregg, and P. Wiles (2009), Sea surface cooling at the equator by subsurface mixing in tropical instability waves, *Nat. Geosci.*, *2*, 761–765.

Moum, J., and J. Nash (2009), Mixing measurements on an equatorial ocean mooring, *J. Atmos. Oceanic Technol.*, *26*, 317–336.

Moum, J., A. Perlin, J. Nash, and M. McPhaden (2013), Seasonal sea surface cooling in the equatorial Pacific cold tongue controlled by ocean mixing, *Nature*, *500*, 64–67, doi:10.1038/nature12363.

Moum, J., and T. Rippeth (2008), Do observations adequately resolve the natural variability of oceanic turbulence?, *J. Mar. Syst.*, *77*, 409–417, doi:10.1016/j.jmarsys.2008.10.013.

Perlin, A., and J. Moum (2012), Comparison of thermal dissipation rate estimates from moored and profiling instruments at the equator, *J. Atmos. Oceanic Technol.*, *29*, 1347–1362.

Rohr, J., E. Itsweire, K. Helland, and C. Van Atta (1988), Growth and decay of turbulence in a stably stratified shear flow, *J. Fluid Mech.*, *195*, 77–111.

Shih, L., J. Koseff, J. Ferziger, and C. Rehmann (2000), Scaling and parameterization of stratified homogeneous turbulent shear flow, *J. Fluid Mech.*, *412*, 1–20.

Smyth, W., and J. Moum (2000), Length scales of turbulence in stably stratified mixing layers, *Phys. Fluids*, *12*, 1327–1342.

Sun, C., W. Smyth, and J. Moum (1998), Dynamic instability of stratified shear flow in the upper equatorial Pacific, *J. Geophys. Res.*, *103*, 10,323–10,337.

Thorpe, S. (1973), Turbulence in stably stratified fluids: A review of laboratory experiments, *Boundary Layer Meteorol.*, *5*, 95–119.

Thorpe, S., and Z. Liu (2009), Marginal instability?, *J. Phys. Oceanogr.*, *39*, 2373–2381.

Thorpe, S., W. Smyth, and L. Li (2013), The effect of small viscosity and diffusivity on the marginal stability of stably stratified shear flows, *J. Fluid Mech.*, *731*, 461–476.

Xie, S.-P. (2013), Climate science: Unequal equinoxes, *Nature*, *500*, 33–34, doi:10.1038/nature12456.